Geophys. J. R. astr. Soc. (1980) **63**, 361–380

A first-order scattering solution for modelling elastic wave codas – I. The acoustic case

P. E. Malin* *Department of Geological and Geophysical Sciences, Guyot Hall, Princeton University, Princeton, New Jersey 08540, USA*

Received 1980 February 13; in original form 1979 February 5

Summary. A corrected, first-order solution for modelling acoustic wave scattering in layered halfspaces containing random inhomogeneities is derived. Energy lost to higher order scattering and intrinsic attenuation is included in the correction, which is constructed so that energy is conserved to first order. The complex propagation effects of the layering are overcome by representing the motion as a sum of normal modes. This approach renders the kinematic description of the scattering two dimensional, with the wave vectors of incident and scattered modes lying parallel to the layering. At each level in the halfspace, the inhomogeneities are resolved into two-dimensional Fourier spectra also parallel to the layering. The root mean square (rms) motion of a scattered mode depends on the correlation between spectra at different levels and the group velocity of the mode. To simplify the solution, it is assumed that the inhomogeneity spectra are piecewise constant and that the energy of a normal model propagates only at its group velocity. The final step of the theory establishes a criterion for the source–receiver separations over which the results are accurate.

Numerical calculations have been carried out for a single layer of inhomogeneities over a halfspace. The spectra of the inhomogeneities were assumed band limited, and several different spectra were examined. The results suggest the existence of a diagonal selection rule whereby a wavelet of mode order n scatters mostly to wavelets of the same order. Moreover, a resonant frequency of scattering occurs, causing the rms signal to appear monochromatic. The frequency of the resonance is controlled by the inhomogeneity spectra band limits. With the aid of the diagonal selection rule, the simplified solution allows for both rapid computation of synthetic signals and inversion of data for scattering cross-section.

Existing data suggest the theory may be applied to obtain approximate models of local earthquake codas. The synthetic signals of the single layer cases, for example, have codas similar to published observations. To illustrate the inversion of data with the theory, a preliminary scattering cross-section for the lunar crust is presented.

* Present address: Department of Geological Sciences, University of Southern California, University Park, Los Angeles, California 90007, USA.

Introduction

Recordings of elastic waves in layered media commonly include long concluding trains, or codas, of oscillatory motion. For seismologists, the most familiar examples are the codas of local earthquakes ($M < 4$ and $\Delta < 100$ km) and lunar seismic events. In these cases, the source of the coda appears to be scattering from random inhomogeneities within crustal and mantle layers (Aki & Chouet 1975; Dainty *et al.* 1974). Various theories for elastic waves in layered media containing inhomogeneities have been given by Herrera & Mal (1965), Kennett (1972), Saastamoinen (1977) and Woodhouse (1974). In this first of two papers, the acoustic case is used to illustrate a first-order, or Born-like, scattering theory for modelling wave motion in such media.

The theory, known as first-order multiple scattering, includes a correction for energy loss to higher order scattering and intrinsic attenuation (for a general review of this and other scattering theories, including cross-section definitions, see Ishimaru 1978; see also Landau & Lifshitz 1959, p. 295). Key features in its application here are the use of normal modes to represent the motion and description of the inhomogeneities by their statistical properties. What is implied by normal modes are waves entirely trapped within the model layers by total reflection (Tolstoy 1973, pp. 95–108; Ewing, Jardetzky & Press 1957, pp. 124–147). Pekeris (1948) has shown that such modes conveniently and compactly contain all possible ray paths between a source and receiver. This representation, however, neglects waves that start out as, or scatter to, waves only partially trapped by the lowest horizon. As will be pointed out in the Discussion, if the layering forms a strong wave trap the resulting errors will not be serious.

Each normal mode is the product of a wave propagating parallel to the layers and a standing wave normal to them. The propagation vectors of incident and scattered waves are thus parallel to the layers, rendering the kinematic description of the scattering two dimensional. Since the inhomogeneities couple the modes, their properties along and normal to the layering are also treated in a separate manner. Parallel to the layers a two-dimensional Fourier representation is utilized (a brief but rigorous treatment of the procedure is given by Tatarskii 1971, pp. 7–10). The character of these spectra and their variation normal to the layering determine the scattering cross-sections between modes. The group velocity of the scattered mode also appears in the cross-section formulae and plays an important role in the scattering process. The spectral description of the inhomogeneities is an extension to three dimensions of the one used by Kennett (1972) in two dimensions.

Along with the theory, the scattering cross-sections and point source signals of some layer over halfspace models are presented. These examples are designed to show how the inhomogeneity spectra control the duration and frequency content of a coda. They also suggest two important features for acoustic wave scattering in layered media. First, for inhomogeneities composed of a limited range of scale lengths, the cross-sections are peaked at a frequency set by the scale-length limits. Second, a normal mode component (order n) of an incident wave will scatter mostly to the same mode (also order n). This latter result constitutes a 'diagonal selection rule' for the scattering of waves trapped in layered structures.

While the acoustic examples are meant to stand on their own merits, it is suggested that they may be viewed as approximations to the vertical components of seismograms. The model densities and P wave velocities were in fact taken from profiles for some local terrestrial and lunar structures (Ewing *et al.* 1957, pp. 147–149; Cooper & Kovach 1974). Shear wave contributions are neglected, but their inclusion does not alter the basic method introduced here (for the complete theory see Malin 1978). Moreover, published observations indicate first-order scattering theory is valid for modelling seismic codas. Support for this

assertion is briefly given below, and the advantages it provides in such modelling are outlined in the Discussion.

First-order theory accurately describes the scattering of waves whenever their wavenumber k, the density of scatterers η and the total scattering cross-section σ^t obey

$$\alpha \ll k, \qquad \alpha \equiv \eta\sigma^t \tag{1}$$

(Chernov 1960, pp. 35–57). By its definition, the scattering coefficient α is the fraction of wave energy lost per unit distance travelled. Equation (1) simply states that first-order theory is accurate when the fractional loss per unit wavelength is much less than 1. The source–receiver distance, d, over which valid results can be obtained is also limited (Bugnolo 1960). For isotropically scattered normal modes the appropriate criterion, derived in the next section, is

$$d \leqslant 1.25\alpha^{-1}. \tag{2}$$

Beyond this distance higher-order scattering must be taken into account.

Aki & Chouet (1975) have determined the backscattering energy loss of local earthquake waves. In the frequency range of 1 to 10 Hz and higher, it is on the order of 10^{-2}–10^{-3} $km^{-1}\,rad^{-1}$. As pointed out by Sato (1977), this parameter is equivalent to the density of scatterers times their differential cross-section in the backward direction: $\alpha(\pi) = \eta\sigma^d(\pi)$. Thus for the wavenumbers Aki & Chouet consider (10^0–$10^2\,km^{-1}$), equation (1) holds for total and backscattering cross-sections differing by as much as an order of magnitude. Since the evidence given by these authors indicates the coda is composed of isotropically scattered waves, first-order models of such waves should be adequate. By equation (2), the maximum source–receiver distance the models can be extended to is 10^2 km.

Dainty & Toksöz (1977) have reported that at 1 Hz the lunar scattering coefficient is similar to that of the Earth. At 10 Hz, they find it exceeds the terrestrial value by an order of magnitude. On the other hand, the corresponding wavenumbers are also an order of magnitude larger. These differences balance and equation (1) remains satisfied. The distance range for accurate first-order modelling at 10 Hz is, however, reduced to 10 km. Beyond this distance a multiple scattering method such as that of Kopnichev (1977) must be used. Later in this paper, a consistent first-order model is constructed for frequencies below 2 Hz and distances less than 10^2 km.

It is significant to note that waves trapped in plane layers have geometric spreading factors of $r^{-1/2}$. The efficiency of such wave propagation is well known: the acoustic stratification of the oceans, for example, allows even small explosions to be heard over distances of 10^4 km (see the discussion of the SOFAR channel in Tolstoy 1973). The equivalent examples in the solid earth are surface waves. Even weak scattering between trapped waves can thus generate a surprisingly large coda.

Basic theory

The aim of this section is to derive equations for modelling the scattering of acoustic waves in layered halfspaces. The general halfspace model under consideration, along with the geometry required for the derivation is shown in Fig. 1. It will be assumed that the density and bulk modulus of this model can be separated into mean values varying normal to the layering plus randomly fluctuating volume components:

$$\begin{aligned} \rho &= \rho_0(z) + \rho_1(x, y, z), \qquad \langle\rho\rangle = \rho_0 \\ \lambda &= \lambda_0(z) + \lambda_1(x, y, z), \qquad \langle\lambda\rangle = \lambda_0. \end{aligned} \tag{3}$$

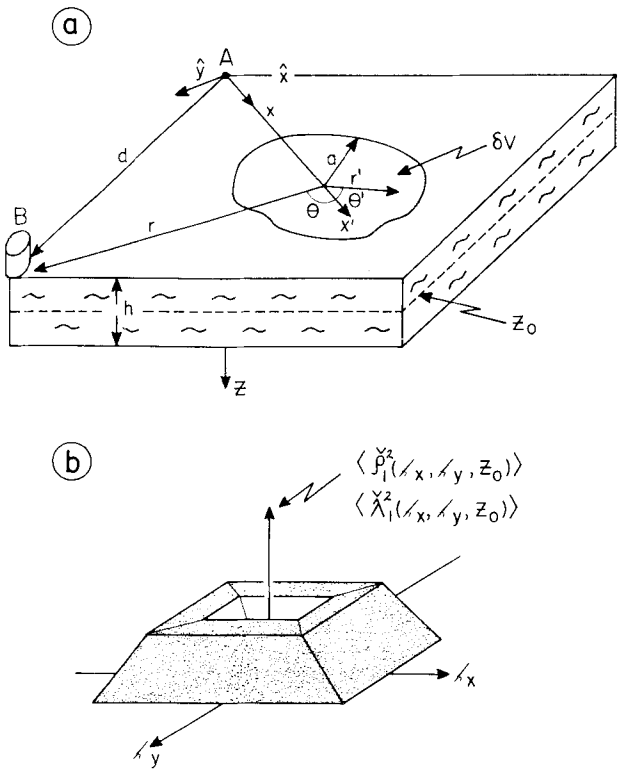

Figure 1. (a) Oblique view of a layered acoustic halfspace with random inhomogeneities in the top layer. This layer is of thickness h and has a source and receiver on its surface at positions A and B respectively (in the theory these positions are arbitrary). Also shown is a subvolume δV of inhomogeneities, which is assumed to be in the far field of the source and receiver, and to have a mean dimension of $2a$ parallel to layering. For convenient calculation of its cross-section, δV was chosen to lie on the $\hat{x}$ axis at x; x' is thus the distance from x along the direction of plane waves from A, θ is the scattering angle, r the distance from x to B and d the source–receiver separation. The coordinates r' and θ' appear in the Green's function of equation (8). This geometry must, of course, be generalized for an arbitrary subvolume. However, once the cross-sections of the inhomogeneities are known, only the source–δV–receiver distances are needed to compute synthetic signals. In the theoretical development the inhomogeneities within δV will be represented in terms of their two-dimensional Fourier spectra parallel to the layering. (b) The two-dimensional Fourier representation of a possible (but arbitrarily chosen) distribution of density or bulk modulus inhomogeneities at the level z_0. It is assumed that $\langle \rho_1 \rangle = \langle \lambda_1 \rangle = 0$ so that $\tilde{\rho}_1(0,0,z) = \tilde{\lambda}_1(0,0,z) = 0$.

Here the ensemble mean value denoted by $\langle \cdot \rangle$ is taken as identical to a spatial average. The elastic displacement $\tilde{\mathbf{u}}$ associated with these properties and an arbitrary source $\tilde{\mathbf{f}}$ are the familiar equations ($\sim$ denoting the frequency domain)

$$
\begin{aligned}
&-\rho\omega^2\tilde{\mathbf{u}} = \nabla\tilde{p} + \tilde{\mathbf{f}} \\
&\tilde{p} = \lambda\,\nabla\cdot\tilde{\mathbf{u}} \\
&\tilde{p} = 0 \quad \text{on} \quad z = 0 \\
&\tilde{\mathbf{u}}\cdot\hat{z} \quad \text{and} \quad \tilde{p} \text{ continuous.}
\end{aligned}
\tag{4}
$$

The first step in dealing with these random differential equations is to convert them into an integral equation. Following Hudson (1977), equation (4) may be written as

$$\tilde{\mathbf{u}} = \int dV \tilde{G} \cdot \tilde{\mathbf{f}} + \int dV [\rho_1 \omega^2 \tilde{G} \cdot \tilde{\mathbf{u}} - \lambda_1 \nabla \cdot \tilde{\mathbf{u}} \nabla \cdot \tilde{G}] = \tilde{\mathbf{u}}^0 + \tilde{\mathbf{u}}^s \tag{5}$$

where $\tilde{G}$ is the Green's function of the mean structure and the layering is assumed flat. This form shows that the inhomogeneities act as sources of motion and the scattered displacement depends on the total field.

Equations such as (5) are traditionally solved iteratively, the total field being first approximated by $\tilde{\mathbf{u}}^0$. The first iteration is adequate when the ratio of the scattered to total field is small. If the inhomogeneities are confined to some finite region distant to the source and receiver, the ratio equals the fraction of an incident plane wave scattered. Thus taking $\tilde{\mathbf{u}}^0$ in the plane wave limit, this 'total scattering cross-section' is defined by

$$\sigma^t \equiv \int d\theta \sigma^d(\theta) \equiv \int d\theta \left[\lim_{r \to \infty} \frac{r \langle \| \tilde{\mathbf{u}}^s \|^2 \rangle}{\| \tilde{\mathbf{u}}^0 \|^2} \right]. \tag{6}$$

The norm $\| \cdot \|$ denotes the total energy density, which for plane waves is equal to twice the kinetic energy density (Landau & Lifschitz 1959, p. 249). The definition anticipates the two-dimensional nature of the wave propagation by assuming the scattered wave energy spreads as r^{-1}. Likewise, the 'differential cross-section' σ^d is assumed to depend on the planar angle θ (see Fig. 1a). The units of σ^t and σ^d are length and length per radian.

In the case at hand, numerous regions of inhomogeneities are assumed to exist, they may even form a continuous layer. The density of scatterers η is defined as the number of regions per unit area parallel to the layering. As stated, if the density of regions times their total cross-sections satisfies equations (1) and (2), the scattered field of each region is accurately given by

$$\tilde{\mathbf{u}}^s \approx \int_{\delta V} dV [\rho_1 \omega^2 \tilde{G} \cdot \tilde{\mathbf{u}}^0 - \lambda_1 \nabla \cdot \tilde{\mathbf{u}}^0 \nabla \cdot G]. \tag{7}$$

A formal justification of this first-order, or Born, approximation may be found in Frisch (1968), as well as Chernov (1960). The volume integral is over the region δV under consideration, where it is assumed that $\langle \rho_1 \rangle = \langle \lambda_1 \rangle = 0$. When equation (7) is used to evaluate the various cross-sections, δV must be in the far field of the source and observation point.

Except for ρ_1 and λ_1, the scattered displacement from δV is now expressed in quantities that depend on the mean properties of the halfspace. Construction of the scattered displacement due to all the regions proceeds from this result. Briefly stated, the remaining steps consistent with first-order theory are: (1) finding convenient representations for $\tilde{G}$, $\tilde{\mathbf{u}}^0$, ρ_1, λ_1 and grinding through the algebra of equation (7); (2) transforming the result into the time domain; (3) choosing a component of this displacement and finding its ensemble mean square value; (4) adding a correction for higher-order scattering and intrinsic attenuation; (5) summing the contributions of each region independently; and finally (6) establishing the distances over which the results are valid.

Step 1. $\tilde{G}$ and $\tilde{\mathbf{u}}^0$ are constructed from the normal modes of the mean halfspace. The modes may be obtained from the equivalent of equation (4) with $\rho_1 = \lambda_1 = 0$ and the added condition $\tilde{\mathbf{u}} \to 0$ as $z \to \infty$. Due to this latter assumption, all incident and scattered waves that do not remain trapped in the layering are neglected. The results below are thus accurate when the ratio of trapped to total wave energy is a first-order quantity (see Discussion).

Reduced to the far field and written in the mixed coordinates of Fig. 1(a), the Green's function and incident displacement are

$$\tilde{G} = r^{-1/2} \sum_n \xi_n \mathbf{R}_n \mathbf{S}_n \exp(i\chi_n) \qquad \tilde{\mathbf{u}}^0 = x^{-1/2} \sum_m \xi_m \mathbf{R}_m s_m \exp(i\chi'_m)$$

$$\xi_n = k^{1/2}(32\pi)^{-3/2}(\omega g_n \Omega_n)^{-1} \qquad \Omega_n = \int dz\, \rho_0 \mathbf{R}_n \cdot \mathbf{R}_n^*$$

$$\mathbf{R}_n = v_n \hat{r} + i w_n \hat{z} \qquad \mathbf{S}_n = v_n \hat{r}' - i w_n \hat{z} \tag{8}$$

$$\chi_n = k_n[r' \cos(\theta - \theta') - r] + \frac{\pi}{4} \qquad \chi'_m = -k_m(x' + x) + \frac{\pi}{4}$$

$$s_m = \int dV \mathbf{S}_m \cdot \tilde{\mathbf{f}} \qquad g_n = n\text{th mode group velocity}$$

v_n, $w_n = n$th mode z dependent eigenfunctions. With this choice of $\tilde{G}$ and $\tilde{\mathbf{u}}^0$, useful representations for ρ_1 and λ_1 are their two-dimensional Fourier spectra parallel to the layering (see Fig. 1b).

$$\begin{bmatrix} \rho_1 \\ \lambda_1 \end{bmatrix} = \int_{-\infty}^{\infty} d\kappa_x\, d\kappa_y \begin{bmatrix} \check{\rho}_1 \\ \check{\lambda}_1 \end{bmatrix} \exp(-i\kappa_x x - i\kappa_y y). \tag{9}$$

As motivation for this step it should be noted that, parallel to the layering, $\tilde{\mathbf{u}}^0$ is also a superposition of sine and cosine functions. Kennett (1972) has applied a similar resolution for two-dimensional inhomogeneities. Note that equation (9) allows for inhomogeneities that are different in the x and y directions. This feature can be carried through the development without great difficulty. Inserting equations (8) and (9) into (7) and exchanging the orders of integration over $d\kappa_x d\kappa_y$ and $dx\, dy$, each term in the double sum for $\tilde{\mathbf{u}}^s$ becomes proportional to

$$\tilde{\mathbf{u}}^s \propto (k_{nx} - k_m - \kappa_x)^{-1}(k_{ny} - \kappa_y)^{-1} \sin[a(k_{nx} - k_m - \kappa_x)] \sin[a(k_{ny} - \kappa_y)] \tag{10}$$

where a is the mean planar radius of δV, k_{nx} and k_{ny} the x and y components of the scattered wave vector, and k_m the incident wave vector, which is taken to be on the x axis. The functions on the right side of equation (10) have their most important contributions to the remaining integrations over $d\kappa_x\, d\kappa_y$ where

$$\mathbf{K}^{\mathrm{B}}_{mn} \equiv (\kappa_x, \kappa_y, 0) = (k_{nx} - k_m, k_{ny}, 0). \tag{11}$$

In fact, if $a|\mathbf{K}^{\mathrm{B}}_{mn}| \gg 1$, contributions at wavenumbers other than $\mathbf{K}^{\mathrm{B}}_{mn}$ can, to first order, be ignored. Equation (11) defines a so called Bragg condition and $\mathbf{K}^{\mathrm{B}}_{mn}$ will be termed the Bragg vector. The scattered displacement then simplifies to

$$\tilde{\mathbf{u}}^s = (rx)^{-1/2} \sum_{mn} \xi_m \xi_n \mathbf{R}_n s_m \int dz\, [\check{\rho}_1 \omega^2 \epsilon_{mn} - \check{\lambda}_1 \zeta_{mn}] \exp(-i\gamma_{mn})$$

$$\check{\rho}_1 = \check{\rho}_1(k_{nx} - k_m, k_{ny}, z) \equiv \check{\rho}_1(\mathbf{K}^{\mathrm{B}}_{mn}, z)$$

$$\check{\lambda}_1 = \check{\lambda}_1(k_{nx} - k_m, k_{ny}, z) \equiv \check{\lambda}_1(\mathbf{K}^{\mathrm{B}}_{mn}, z) \tag{12}$$

$$\epsilon_{mn} = (v_m v_n \cos\theta - w_m w_n)$$

$$\zeta_{mn} = (k_m v_m - \partial_z w_m)(k_n v_n - \partial_z w_n)$$

$$\gamma_{mn} = k_n r + k_m x - \frac{\pi}{2}.$$

Step 2. In this step the approximate method of Aki (1960) is used to return equation (12) to the time domain. Aki's method breaks the transform integral into segments over which only the phase of the integrand is rapidly varying. Expressed in compact notation, each term of $\tilde{\mathbf{u}}^s$ yields for the jth segment of width $\delta\omega_j$

$$\frac{1}{2\pi}\int_{\delta\omega_j} d\omega[\![\psi \exp[-i(\gamma-\omega t)]]\!]_{mn} = \frac{1}{2\pi}\left[\psi \frac{\sin \delta\omega\bar{t}}{\bar{t}} \exp[-i(\gamma-\omega t)]\right]_{mnj}$$

$$\bar{t}_{mnj} = \left[\frac{r}{g_n} + \frac{x}{g_m} - t\right]_j . \tag{13}$$

Here ψ represents all the coefficients on the right side of equation (12), which are assumed constant over each transform segment. From equation (13), it can be seen that $\mathbf{u}^s$ is once again relatively large over a narrow range of its independent variables, namely where $\bar{t}_{mnj} = 0$ for $(r/g_n + x/g_m)\delta\omega \gg 1$. The times for which $\bar{t}_{mnj} = 0$ correspond to the arrival of energy at the group velocities of incident and scattered waves. In the subsequent steps, energy propagating at other speeds will be neglected. The condition $\bar{t}_{mnj} = 0$ places no restrictions on the time behaviour of the source.

Step 3. Taking the ith displacement component of $\mathbf{u}^s$, squaring it and averaging, the expected signal is ultimately found to depend on the various mean products of $\check{p}_1$ and $\check{\chi}_1$. These products are: $\langle \check{p}_1 \check{p}_1' \rangle$, $\langle \check{p}_1 \check{\chi}_1' \rangle$ and $\langle \check{\chi}_1 \check{\chi}_1' \rangle$, where unprimed and primed quantities depend on $(\mathbf{K}^B_{mnj}, z)$ and $(\mathbf{K}^B_{opl}, z')$ respectively. Under the condition $a|\mathbf{K}^B_{mn}| \gg 1$, only the products with $\mathbf{K}^B_{mnj} = \mathbf{K}^B_{opl}$ are non-negligible (Tatarskii 1971, p. 9). Equivalently, it will be assumed that the spectral amplitudes of the inhomogeneities at different wavenumber are uncorrelated. The Bragg vectors $\mathbf{K}^B_{mnj}$ and $\mathbf{K}^B_{opl}$ are clearly equal whenever $m = o$, $n = p$ and $j = l$. Cases where the Bragg vectors are equal but $m \neq o$, $n \neq p$ and $j \neq l$ (or any combination of equal and unequal indices) can arise. However, the added requirement that $\bar{t}_{mnj} = \bar{t}_{opl} = 0$ makes these cases fortuitous and they will be neglected. The geometrical construction introduced in the next section can be used to visualize these relations.

The products $\langle \check{p}_1 \check{p}_1' \rangle$ etc. may now be expressed as the correlation functions $\Gamma_{\rho\rho}(\mathbf{K}^B_{mnj}, z, z')$. To simplify numerical evaluations involving these correlations, they will be approximated by piecewise constant functions:

$$\Gamma_{\rho\rho}(\mathbf{K}^B_{mnj}, z, z') = \sum_q \mathrm{P}_q^2(z, z')\Pi_q(\mathbf{K}^B_{mnj}). \tag{14}$$

Here Π_q is 1 if $k_{(q-1)x} < \kappa_x < k_{qx}$ and $k_{(q-1)y} < \kappa_y < k_{qy}$ and zero otherwise. The inhomogeneity spectrum illustrated in Fig. 1(b) has thus been broken into box cars of the sort shown in Fig. 2. Each segment describes perturbations of equal magnitude and z-dependent correlation, but different x and y length-scales. Other definitions of Π_q can also be made. A more useful form might for example be $\Pi_q = 1$ if $|k_{q-1}| < |\mathbf{K}^B_{mnj}| < |k_q|$, and zero otherwise. In either case, the z component mean square displacement due to δV at $\bar{t}_{mnj} = 0$ is now given by

$$\langle |u_z^s|^2 \rangle = (rx)^{-1} \sum_{mnjq} Q^2_{mnj} I_{mnjq}$$

$$Q_{mnj} = (2\pi)^{-1}[\xi_m \xi_n \mathbf{R}_n \cdot \hat{z}\, s_m \delta\omega]_j$$

$$I_{mnjq} = [\omega^4(\cos^2\theta I_1 + 2\cos\theta I_2 + I_3) - \omega^2(\cos\theta I_4 + I_5) + I_6]_{mnjq} \tag{15}$$

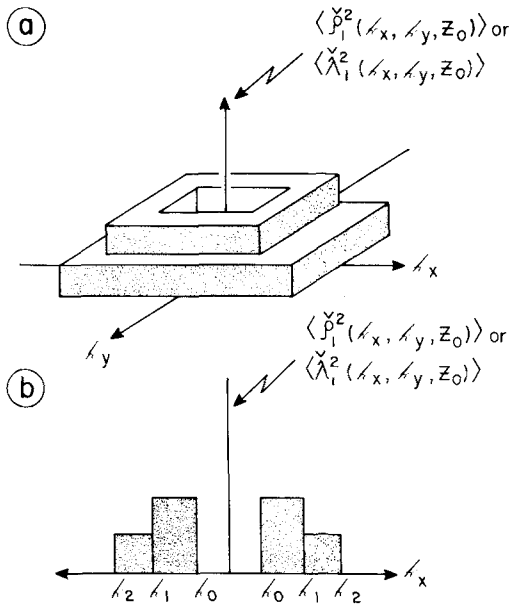

Figure 2. (a) Piecewise constant approximation to the two-dimensional Fourier distribution shown in Fig. 1(b). In this case the spectrum has been approximated with box car like functions parallel to the k_x and k_y axes. (b) A cross-section along the k_x axis through the box cars. The accuracy of the representation can be improved by increasing the number of box cars.

$$\begin{bmatrix} I_1 \\ I_2 \\ I_3 \\ I_4 \\ I_5 \\ I_6 \end{bmatrix}_{mnjq} = \Pi_q \int_0^\infty dz\, dz' \begin{bmatrix} v_m v_n v'_m v'_n \mathrm{P}_q^2 \\ v_m v_n w'_m w'_n \mathrm{P}_q^2 \\ w_m w_n w'_m w'_n \mathrm{P}_q^2 \\ v_m v_n \zeta'_{mn} (\mathrm{P}\Lambda)_q \\ w_m w_n \zeta'_{mn} (\mathrm{P}\Lambda)_q \\ \zeta_{mn} \zeta'_{mn} \Lambda_q^2 \end{bmatrix}_j$$

Step 4. A correction, or renormalization, for the scattering regions that lie in the paths of the incident and scattered waves can be included in equation (15). The renormalization will be achieved by reducing, to first order, these waves in proportion to the inhomogeneities they encounter. A similar scheme has been employed by Sato (1977). It is important to note that the requirement $\langle \rho_1 \rangle = \langle \lambda_1 \rangle = 0$ makes this correction consistent to first order. Under this condition no energy can recombine with the incident wave, as can be seen from the Bragg vector $\mathbf{K}^{\mathrm{B}}_{mnj}$. For such an event, $\mathbf{K}^{\mathrm{B}}_{mnj} = 0$. Since $\check{p}_1(0, z) = \check{\lambda}_1(0, z) = \langle \rho_1 \rangle = \langle \lambda_1 \rangle = 0$ then $\tilde{\mathbf{u}}^{\mathrm{s}} = 0$ also. Without $\langle \rho_1 \rangle = \langle \lambda_1 \rangle = 0$ the wave incident on a region would not be the direct wave minus the energy lost to first-order scattering.

From the definition of the scattering coefficient α, for each unit distance travelled by the mth mode incident or scattered wavelet

$$\begin{aligned} \delta \langle |\mathbf{u}_m|^2 \rangle &= -\alpha_m \langle |\mathbf{u}_m^0|^2 \rangle \delta r \\ \langle |\mathbf{u}_m|^2 \rangle &= \langle |\mathbf{u}_m^0|^2 \rangle \exp(-\alpha_m r) \end{aligned} \qquad (16)$$

where $\langle|\mathbf{u}_m^0|^2\rangle$ is the initial mean square wavelet. Equation (6) may be used to find α_m with the total energy density given to first order by

$$\langle\|\tilde{\mathbf{u}}\|^2\rangle = \omega^2 \int dz\, \rho_0 \langle\tilde{\mathbf{u}} \cdot \tilde{\mathbf{u}}^*\rangle. \tag{17}$$

Using steps 1 and 3, α_m is equal to

$$\alpha_m = \eta \cdot \sum_{nq} \xi_n^2 \frac{\Omega_n}{\Omega_m} \int_0^{2\pi} d\theta\, I_{nmq} = 2\eta \sum_{nq} \xi_n^2 \Omega_n \Omega_m^{-1} \Theta_{mnq}$$

$$\Theta_{mnq} = \{\omega^4[(\theta + \tfrac{1}{2}\sin\theta)I_1 + 2\sin\theta I_2 + \theta I_3] + 2\omega^2[\sin\theta I_4 + \theta I_5] + \theta I_6\}_{mnq}^{\theta_q} \tag{18}$$
$$\theta_{q-1}$$

The index n is over all the possible modes to which the mth mode can scatter. Since this calculation is carried out in the frequency domain, the j index is fixed and implicitly included. The limits θ_{q-1} and θ_q depend in turn on the k_{q-1} and k_q of equation (14) and Fig. 2 (this relation will be discussed below and in the Appendix). According to equation (18), α_m is a function of group velocity as well as the inhomogeneities. Thus the mean, layered model enters directly into the description of the scattering.

For the observations discussed in the Introduction, wave energy losses due to intrinsic attenuation appear as important as those due to scattering. Such dissipation may also be included in each layer of the model in Fig. 1. If $\tau(z)$ is the attenuation factor at the depth z then, following Anderson & Archambeau (1964), the net attenuation of the mth normal mode is

$$\tau_m = \Omega^{-1} \int_0^{\infty} dz\, \tau(z)\,[v_m^2 + w_m^2]. \tag{19}$$

Adding this to α_m the net energy loss per unit distance is $\bar{\alpha}_m = \alpha_m + \tau_m$. Finally, equation (14) may be corrected so that at $\bar{t}_{mnj} = 0$

$$\langle|\mathbf{u}_z^s|^2\rangle = (rx)^{-1} \sum_{mnjq} Q_{mnjq}^2 I_{mnjq} \exp(-\bar{\alpha}_m x - \bar{\alpha}_n r). \tag{20}$$

Step 5. Sufficient theoretical ammunition is now available for finding the signal due to all the inhomogeneities. It will be accomplished by summing the mean square signals of the regions. This step requires that the signals of each region be uncorrelated, or equivalently the regions must be much larger than the longest scale-length inhomogeneity. (In terms of the spectra of Fig. 2, the mean scale a must satisfy $k_0 a \gg 1$.) For each region the signal per unit area parallel to layering is $(\pi a^2)^{-1}\langle|\mathbf{u}^s|^2\rangle$. The net signal, including renormalization of the direct wave, equals

$$\langle|u_z|^2\rangle \approx (u_z^0)^2 + (\pi a^2)^{-1} \int_A dA\, \langle|u_z^s|^2\rangle. \tag{21}$$

The domain A is the entire xy area over which ρ_1 and λ_1 are non-zero. Next, the condition $\bar{t}_{mnj} = 0$ can be used to simplify equation (20). At a fixed time, only certain values of x and r satisfy $\bar{t}_{mnj} = 0$: they form an ellipse in the xy plane. The areal integral in equation (20) therefore collapses into a line integral. For a point source consisting of a vertical impulse or explosion, this line integral can be computed in terms of logarithmic functions and exponential integrals. The logarithmic contributions arise from the scattering of mth mode wavelets to wavelets of the same order ($n = m$ in equation 20). In a subsequent

section, it will be numerically established that these terms dominate in single layer over halfspace models. Hence, for many important geophysical circumstances involving impulsive or explosive sources, the right hand term of equation (20) is equal to

$$2(\pi a^2)^{-1} \sum_{mjq} Q_{mm}^2 \exp(-\bar{\alpha}_m g_m t)[\omega^4(\phi_3 I_1 + \phi_2 I_2 + \phi_1 I_3) + 2\omega^2(\phi_2 I_4 + \phi_1 I_5) + \phi_1 I_6]_{mmj} \tag{22}$$

where the expressions for ϕ_1, ϕ_2 and ϕ_3 are written out in the Appendix. Again, the integration limits are determined by the box cars of equation (14) and Fig. 2.

Step 6. Since the first-order solution exponentially loses energy to multiple scattering, beyond some distance these contributions cannot be ignored. Following Bugnolo (1960), a useful measure is the distance where one half the total energy has been scattered twice. From Bugnolo, the energy density at the point **R** after n scattering is given by

$$\mathbf{B}_n(\mathbf{R}) = (2\pi)^{-2} \int_{-\infty}^{\infty} d\mathbf{s} \exp(-i\mathbf{s}\cdot\mathbf{R}) q_n(\mathbf{s})$$

$$q_n(s) = \prod_{l=1}^{n} \int_{-\infty}^{\infty} d\mathbf{r} \exp(i\mathbf{r}\cdot\mathbf{s}) \beta_l(\mathbf{r}) \tag{23}$$

$\beta_l(\mathbf{r})$ describing how energy is distributed by the lth scattering. For isotropically scattered normal modes each scattering is equivalent and given by

$$\beta_l(\mathbf{r}) = (2\pi r)^{-1} \alpha_m \exp(-\alpha_m r). \tag{24}$$

The quantity sought is the energy arriving at distance d that has been scattered twice, which is given by

$$\mathbf{P}_2(d) = \int_0^d d\mathbf{R}\, \mathbf{B}_2 = 1 - \alpha_m d \Re_1(\alpha d). \tag{25}$$

In equation (25) $\Re_1$ represents the modified Bessel function of order 1. The criterion that this energy be less than one-half demands that

$$d \leqslant 1.25\alpha^{-1}. \tag{26}$$

A geometrical interpretation

An extremely useful set of geometric relations can be constructed to describe the scattering of the mth mode wavelet due to the qth box car of perturbations. The construction is done at a fixed frequency and is illustrated in Fig. 3. First, concentric circles with radii equal to $|k_m|$, $m = 1, 2, \ldots, p$ are drawn in the wavenumber equivalent of the xy plane (only upper half planes will be included in the figures). The propagation direction and wavenumber of the mth mode can then be indicated by a vector along one of the radii. An example is the first mode with wave vector $k_1\hat{x}$. Further, the scattering of mth mode to the nth may be represented by the incident and scattered wave vectors, the scattering angle between them, and the Bragg vector that is equal to their difference. Such an event will be given the symbolic notation $m \to n$, $\mathbf{K}_{mn}^{\mathrm{B}} = \mathbf{k}_m - \mathbf{k}_n$ and an example is the event $1 \to 1$, $\mathbf{K}_{11}^{\mathrm{B}} = k_1\hat{x} - k_1\hat{y}$, which is shown in Fig. 3(a).

The scattered amplitude of an $m \to n$ event depends on the correlation functions of equation (14). The contribution from the qth box car will, for example, be zero if $\mathbf{K}_{mn}^{\mathrm{B}}$ lies

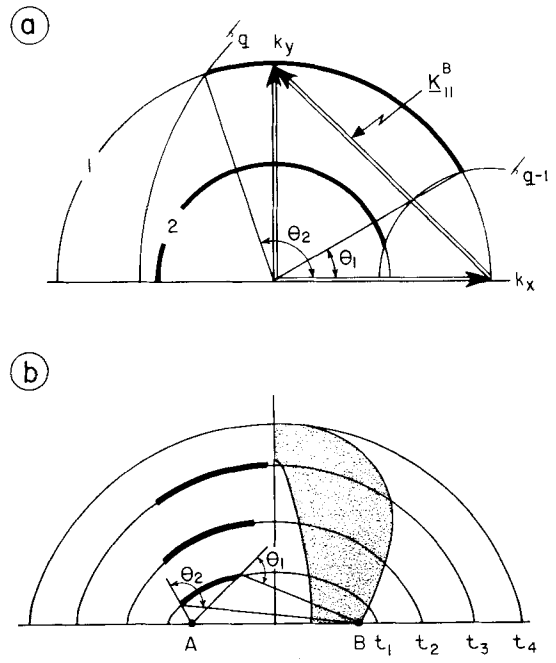

Figure 3. (a) The wavenumber diagram of the normal modes used to represent the wave motion. The diagram is at a frequency where two normal modes are above cut-off: their horizontal wavenumbers $|k_1|$ and $|k_2|$ are equal to the radii of the semi-circles shown. Since the directions of k_x and k_y correspond to those of $\hat{x}$ and $\hat{y}$ in xy space, the propagation direction and order of a mode can be indicated by a vector from the origin to the appropriate circle. An example is the fundamental mode propagating in the $\hat{x}$ direction, $k_1\hat{x}$. The effects of the qth box car of inhomogeneities on this mode can be seen by drawing circles of radii $|k_{q-1}|$ and $|k_q|$ from its head. As the heavy lines indicate, $k_1\hat{x}$ may scatter only into modes whose wave vectors lie within the limits set by $|k_{q-1}|$ and $|k_q|$. For mode 1 to 1 scattering (denoted by $1 \rightarrow 1$), these limits correspond to the scattering angles θ_1 and θ_2. A scattering event may also be described by its 'Bragg vector', $\mathbf{K}^B_{mn}$, equal to the difference of the incident and scattered mode wave vectors. Thus the event shown by double line vectors is determined by the Bragg vector $\mathbf{K}^B_{11} = k_1\hat{x} - k_1\hat{y}$. (b) The xy space equivalent to the wavenumber diagram for $1 \rightarrow 1$ events at various times t. A source and receiver are at A and B respectively, and the curves at times t_1, t_2, t_3 and t_4 are determined by the condition $\bar{t}_{11} = 0$. As illustrated on the left side of the figure, only curve segments within the angles θ_1 and θ_2 contribute signals. The area swept out by these segments is shown by the stipling on the right hand side. At this frequency the area is finite, resulting in a signal of finite duration. The wavenumber diagram shows that this would not be the case for the events $1 \rightarrow 2$.

outside the limits set by the definition of $\Pi_q(\mathbf{K}^B_{mn})$. These limits may be expressed on the wavenumber diagram by tracing out curves on which the minimum and maximum values of $\mathbf{K}^B_{mn}$ lie. The curves must be centred on the head of $\mathbf{k}_m$ and will intersect the mode circles at various points. Only the circle segments between these curves are associated with non-zero scattering amplitudes. The scattered wave vector $\mathbf{k}_n$ must terminate on such a segment for the event $m \rightarrow n$ to be non-zero. An example of this construction for $\Pi_q = 1$ when $|k_{q-1}| < |\mathbf{K}^B_{mn}| < |k_q|$ and zero otherwise is shown in Fig. 3(a). The incident wave was chosen to be $k_1\hat{x}$ and circles of radii k_{q-1} and k_q are centred on it. Heavy lines indicate the circle segments on which scattering can occur. The illustrated event $1 \rightarrow 1$, $\mathbf{K}^B_{11} = k_1\hat{x} - k_1\hat{y}$ is thus non-zero.

Next the events $m \rightarrow n$ can be traced in ordinary xy space. Again, the construction is done at a fixed frequency with the added condition that $\bar{t}_{mnj} = 0$. At time t_l events such as $m \rightarrow n$ lie on the curve $r/g_n + x/g_m = t_l$. The curve segments on which non-zero scattering occurs

correspond to those of the wavenumber diagram. The xy equivalent of the $1 \rightarrow 1$ events in Fig. 3(a) are plotted in Fig. 3(b). For this example only a finite area of the xy plane contributes to the scattering. The signal duration of $1 \rightarrow 1$ events at this frequency is thus also finite. The events $1 \rightarrow 2$, on the other hand, would be non-zero over the entire plane as $t_l \rightarrow \infty$.

The characteristics of these diagrams differ at higher and lower frequencies. At very low frequencies only the fundamental mode ($m = 1$) can satisfy the trapped wave condition. The wavenumber diagram consists of one circle which may lie entirely outside the limits of Π_q. With increasing frequency the first mode circle expands, more modes appear, and the bounds set by Π_q may be reached. For the example in Fig. 3(a), the scattering amplitude of the event $1 \rightarrow 1$, $\mathbf{K}_{11}^{B} = k_1\hat{x} - k_1\hat{y}$ may become equal to zero. At very high frequencies, only events nearly parallel to $\hat{x}$ will be non-zero. (The scattering is mostly 'forward'.) It should be noted, however, that as long as k_{q-1} is finite, no scattering directly parallel to $\hat{x}$ occurs for the $m \rightarrow m$ events. This is an important feature since it insures that the renormalization scheme used in the theory is consistent to first order. The requirement that $\langle \rho_1 \rangle = \langle \lambda_1 \rangle = \check{\rho}_1(0, z) = \check{\lambda}_1(0, z) = 0$ guarantees this consistency. Stated otherwise, the incident wave has not been over corrected by the renormalization since $m \rightarrow m$ scattering in the forward direction does not occur.

The diagonal selection rule

Near the surfaces of the Earth and Moon, compressional wave velocities and densities increase rapidly with depth. This increase generally continues, but is more gradual, through-

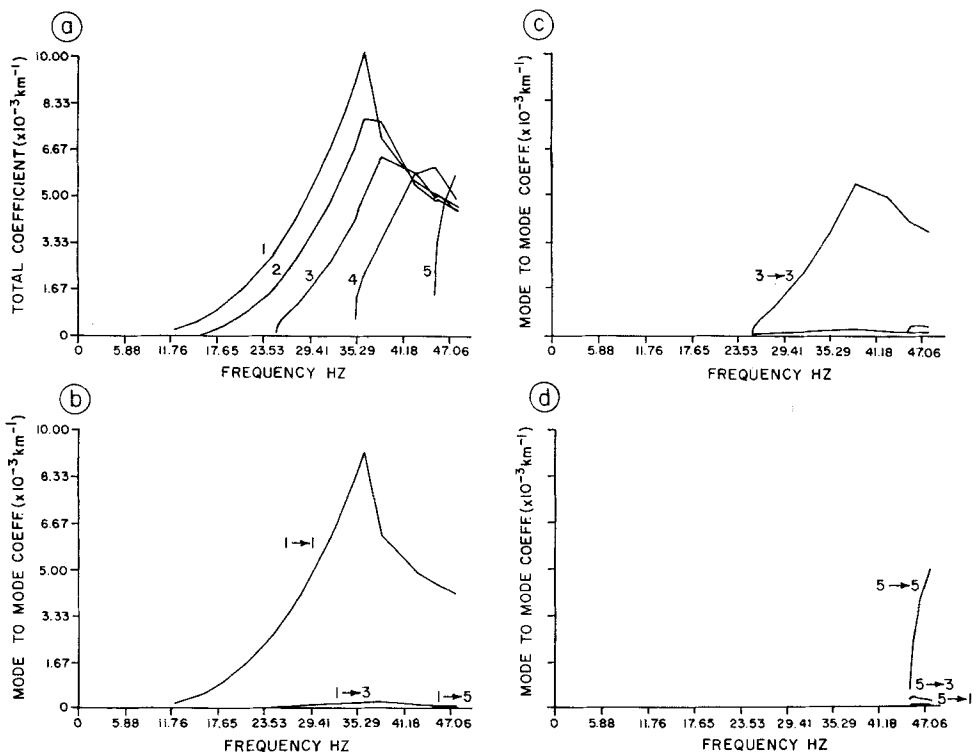

Figure 4. (a) The total scattering coefficients α_m for five normal modes of model 1 (listed in Table 1), (b)–(d), the coefficients α_{mn} for the individual events $m \rightarrow n$. Only the odd events are shown.

out the respective crusts. An appropriate first-order model for these examples is a layer over a halfspace of greater velocity and density. The normal modes of such models obey scaling laws that show that the results of a single case are quite general (Andrianova *et al.* 1967; Ewing *et al.* 1957). For example, models of differing layer thickness and equivalent ratios of material properties have modes that differ by simple scale factors. Thus, while the theory discussed so far allows for more complex structure, the two-layer halfspace covers a variety of situations occurring in nature. Most importantly, the various scattering coefficients of an inhomogeneous layer over a faster and denser halfspace establish a 'diagonal selection rule'. By this rule the events $m \to m$ dominate the scattered signal and the scattering coefficient of equation (18) becomes

$$\alpha_m \approx 2\eta\xi_m^2 \sum_q \Theta_{mmq}. \tag{27}$$

A second facet of such models is that a peak frequency of scattering exists for narrow band $\check{\rho}_1(\mathbf{K}^{\mathrm{B}}_{mn}, z)$ and $\check{\lambda}_1(\mathbf{K}^{\mathrm{B}}_{mn}, z)$. These results will be substantiated below with a series of numerical examples.

The canonical two layer halfspace adopted for examination is that of Ewing *et al.* (1957, p. 147). The specific mean structures chosen are listed in Table 1. The random inhomogeneities were distributed uniformly throughout the upper layer. To calculate the scattering coefficients, correlation functions of the sort used by Aki & Chouet (1975) were assumed:

$$P_q^2(z, z') = P_q^2 \exp(-|z - z'|\mu^{-1}) \tag{28}$$

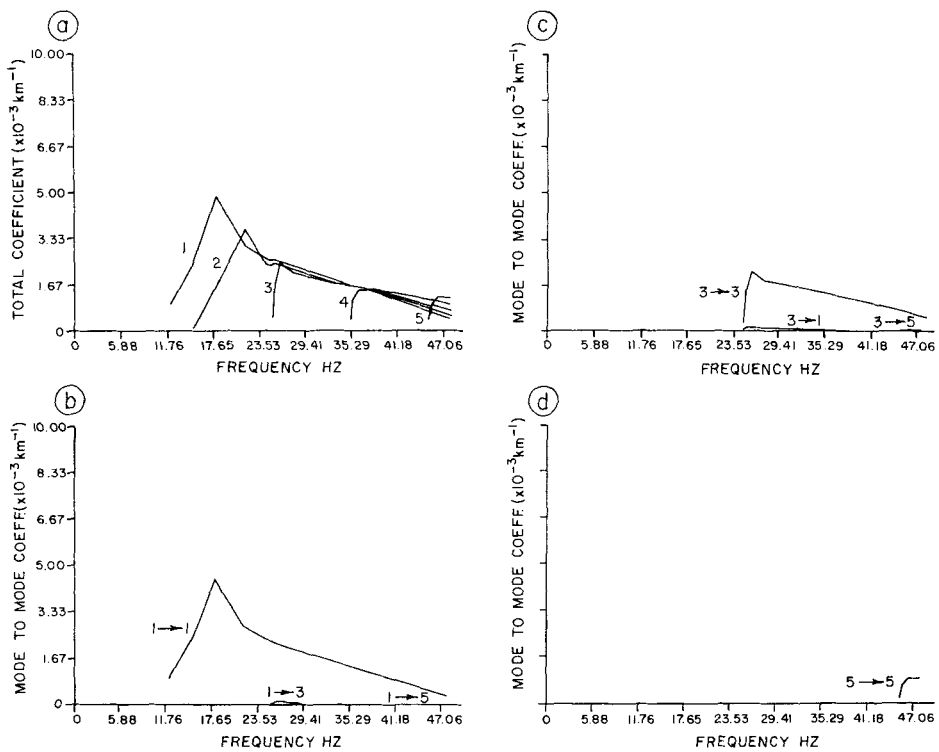

Figure 5. (a)–(d) The same as Fig. 4 but for the second model of Table 1. Again note that $\alpha_m \approx \alpha_{mm}$ and the new position of the fundamental mode resonance.

Table 1. Material properties of the models used to compute the results in Figs 4–8. The percentage variation of λ_1, etc. is given by the parameter δ.

		Models from Ewing *et al.* (1957)			Model from Cooper & Kovach (1974)	
Upper layer		Mean properties	Model 1	Model 2	Mean properties	Model 3
h	km	0.1			1.4	
ρ_0	g cm^{-3}	1.0			2.4	
λ_0	10^{-10}g cm^{-1}s^{-2}	2.25			2.4	
υ_0	km s^{-1}	1.5			1.0	
δ	per cent		30	30		10
$\not{k}_0$	km^{-1}		70.0	70.0		2.0
$\not{k}_1$	km^{-1}		300.0	150.0		30.0
μ	km		0.2	0.2		0.5
Lower layer						
h	km	∞			∞	
ρ_0	g cm^{-3}	2.0			2.8	
λ_0	10^{-10}g cm^{-1}s^{-2}	10.12			44.8	
υ_0	km s^{-1}	2.25			4.0	

with the box car Π_q defined as one if $|\not{k}_{q-1}| < |K^B_{mn}| < |\not{k}_q|$ and zero otherwise. This choice is considered arbitrary since it was not made with some particular case in mind. Furthermore, because more complicated models may be obtained by superposition, only results for a single box car of inhomogeneities were computed ($q = 1$ and $|\not{k}_0| < |K^B_{mn}| < |\not{k}_1|$). Over a range of μ, $|\not{k}_0|$ and $|\not{k}_1|$ values it was found that the scattering coefficients are most sensitive to changes in $|\not{k}_1|$. Two examples with different $|\not{k}_1|$ values, which are listed in Table 1 along with $|\not{k}_0|$ and μ, are illustrated in Figs 4 and 5. Each figure is divided into four panels, the first of which shows the α_m of equation (18) for all the modes between 0 and 50 Hz. The frequency at which these coefficients peak should be noted. In the remaining panels the coefficients representing energy scattered from the mth mode to just the nth mode are plotted (for clarity only the odd terms are plotted). Denoting the latter by α_{mn}, it can be immediately seen that $\alpha_m \approx \alpha_{mm}$, which is the equivalent of equation (27). This diagonal selection property was found to hold even in the limits $\mu \to 0$, $\mu \to \infty$, $|\not{k}_0| \to 0$ and $|\not{k}_0| \to |\not{k}_1|$. The scattering coefficients also maintain their resonance curve like character. While not affecting the diagonal selection rule, changes in $|\not{k}_1|$ produce changes in the position of the resonance peak. As the figures show, a factor of 2 change in $|\not{k}_1|$ results in a similar variation in the resonance frequency of the fundamental mode. It should be noted that $\alpha_m \ll k_m$ for both cases.

Some synthetic seismograms

Synthetic seismograms due to vertical impulses or explosions in the models of Table 1 can now be calculated with either equations (21) or (22). As an example, signals computed with equation (21) will be presented to illustrate the vertical rms motion due to an explosion in the upper layer of the second model. All the modes in the frequency band 0–50 Hz were included in the signals. The intrinsic attenuation was set equal to zero, so that at distances of several hundred kilometres or less the conditions of equations (1) and (2) are satisfied (see Fig. 5). The envelopes of $\langle |u_z|^2 \rangle^{1/2}$ shown in Fig. 6 demonstrate that a substantial coda

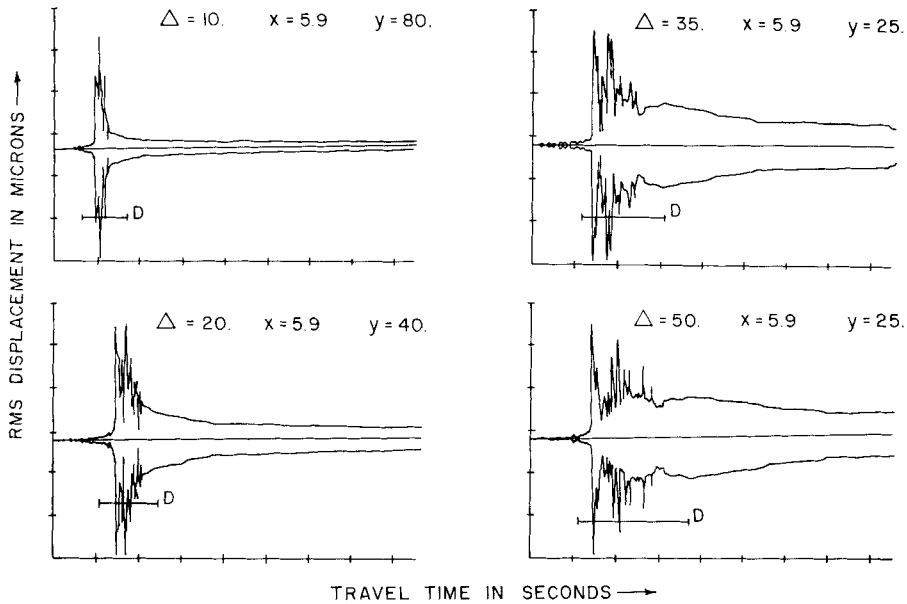

Figure 6. Synthetic seismogram envelopes observed at four distances from an explosion at the middle point of the upper layer of model 2, Table 1. The distances, time and rms displacement scale increments are given in the upper line of each plot by Δ in km, x in s, y in microns respectively. The source strength was arbitrarily scaled so that the y increments would be in microns. The time range of energy arriving on direct paths is indicated by a heavy bar and the letter D. Note that the coda shape remains nearly constant as a function of distance.

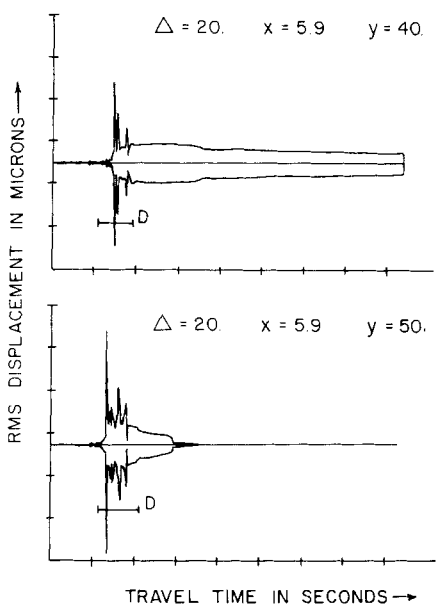

Figure 7. Synthetic seismogram envelopes in different frequency bands for the signal shown in Fig. 6 at Δ = 20 km. The upper plot is for the band 10–15 Hz, the lower for 20–25 Hz. Note how dominant forward scattering reduces the duration of the coda at the higher frequency.

follows the direct arrivals. Adjusting for scale changes, the shape and duration of the coda at the various distances is remarkably constant. Over observation distances many times the layer thickness, the direct waves have undergone normal dispersion. Combined with the coda, a slowly emergent and decaying seismogram results. Observation of such motion hinges on the assumption of zero anelastic energy loss.

In Fig. 7 the rms motion in two separate frequency bands for the same model are plotted. The bands were from 10 to 15 Hz and 20 to 25 Hz. As discussed in the geometric interpretation, at low frequencies $|\boldsymbol{k}_1|$ does not limit the scattering angle: the coda is long and dominated by the resonance frequency shown in Fig. 5. At higher frequencies $|\boldsymbol{k}_1|$ limits the scattering to the forward direction: a short, broadband coda is generated. For the simple box car spectrum of this case, the value of $|\boldsymbol{k}_1|$ clearly plays a deciding role in the character of the coda.

The rms vertical displacement of a third model, listed separately in Table 1, is presented in Fig. 8(a). The velocity and density structure of this case were taken from the lunar model

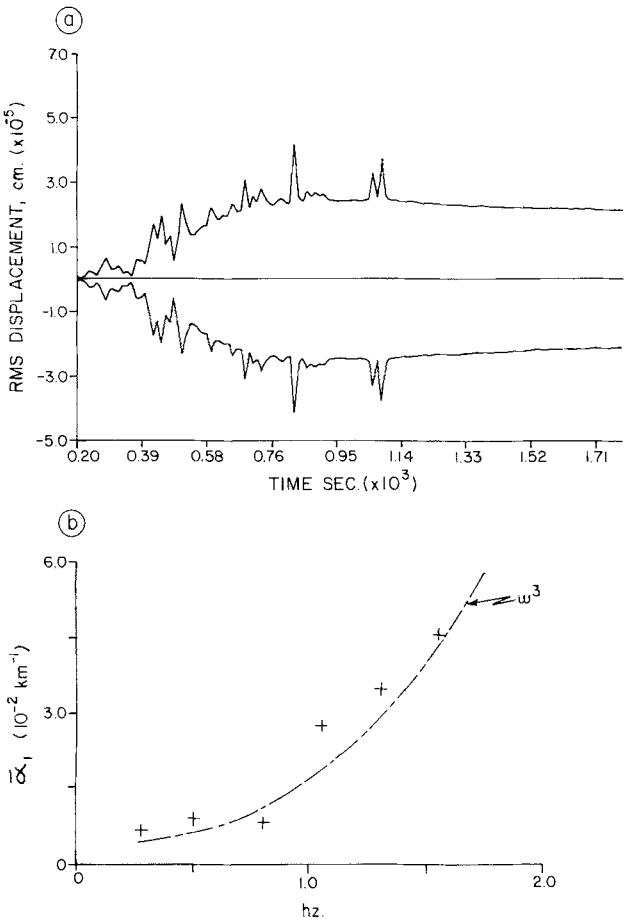

Figure 8. (a) The synthetic seismogram envelope due to a vertical impact on the surface of model 3, Table 1. The observation distance was 400 km. (b) A preliminary determination of the fundamental mode scattering coefficient of the lunar crust. The values of $\bar{\alpha}_1$ were obtained by fitting the coda generated by the Lunar Module 14 impact at 67 km from *Apollo 14* seismometers. It should be noted that $\bar{\alpha}_1$ includes the effects of intrinsic attenuation and meets the first order scattering criteria $\bar{\alpha}_1 \ll k$ and $d \leqslant 1.25\alpha_1^{-1}$. Also plotted is a curve proportional to the frequency cubed.

of Cooper & Kovach (1974). A vertical impulse was assumed for the source. This case shows the effects of large contrasts in the velocities of the two layers. Over a distance–layer thickness ratio equal to the furthest shown in Fig. 6, the direct wave is far more dispersed (the layer velocity is less than that of models 1 and 2). Scattered waves now mix in with the direct waves to produce a very emergent and long lasting coda. The lack of intrinsic attenuation is central to observation of such signals.

Discussion

A crucial feature of the normal mode scattering method is the inclusion of wave propagation effects generated by the layering. It also provides a way of computing the scattering cross-sections used in empirical methods such as those of Aki & Chouet (1975), and Dainty & Toksöz (1977). A weakness in the theory is the use of only trapped waves to represent the motion. This approximation neglects both the positive and negative contributions of scattering between trapped and untrapped waves. Since untrapped to trapped wave scattering occurs basically near the source and the reverse everywhere, the rms motion is overestimated. Errors introduced by this approximation are thus least in strongly trapping models. If in the mean model the fraction of energy in the untrapped waves is much less than one, then the fraction generated by the inhomogeneities is also likely to be small. (Each point in the inhomogeneous medium can be viewed as a source.)

The diagonal selection rule is by far the most useful result presented in this paper. As a consequence of this rule, whenever a layer of weak scatterers is excited by a normal mode, the scattered waves are mostly of the same mode. The frequency of the most strongly scattered waves is controlled by the distribution of inhomogeneity scale sizes parallel to the layering. For a given distribution and mean velocity structure, characteristic scattering coefficients exist for each mode. These coefficients and the diagonal selection rule can be used to rapidly compute the expected motion generated by an impulsive or explosive source within the model.

In models where both diagonal selection and isotropic scattering apply, the coda of the mth mode in the jth frequency band is roughly given by

$$\langle |u_z|^2 \rangle_{mj} \approx \left[q_{mm}^2 \ln\left(\frac{g_m t + d}{g_m t - d}\right) \exp\left(-\bar{\alpha}_m g_m t\right) \right]_j . \tag{29}$$

This result can be derived from equation (21) by setting $\sigma^{\mathrm{d}}(\theta) \approx \sigma^{\mathrm{t}}/2\pi$ and is valid at times and distances where $\bar{\alpha}_m g_m t \ll 1$ and $g_m t > d$. A similar relation has been obtained by Sato (1977) for unlayered models. Equation (29) becomes useful in circumstances where a given source strongly excites a single normal mode. The coda predicted by this equation varies only slightly with distance and reflects the mean velocity–density structure as well as the inhomogeneities.

If the mean structure of an area is known (by refraction studies, say) and a single mode dominates a coda observation, the coefficient $\bar{\alpha}_m$ can be determined inversely. For least-squares fitting, the logarithm of equation (29) is needed:

$$\ln \langle |u_z|^2 \rangle \approx \left[C_{mm} + \ln \ln\left(\frac{g_m t + d}{g_m t - d}\right) - \bar{\alpha}_m g_m t \right]. \tag{30}$$

Aki & Chouet (1975) have analysed local earthquake codas with an empirically derived equation not unlike equation (30). Their method, however, contains no distance dependence and combines the group velocity and scattering coefficient into a single parameter. The

relationship of the latter parameter to the mean structure, inhomogeneities and attenuation implied by equation (30) is not known.

On the other hand, Mark & Sutton (1975) have demonstrated that mostly fundamental mode waves compose the coda generated by the Lunar Module impact of *Apollo 14*. Using their crustal model and the displacement spectra computed by Nakamura (1978), the coefficient α_1 was modelled with equation 30. The values of α_1 between 0 and 2 Hz are plotted in Fig. 8(b). Over these frequencies equations (1) and (2) are satisfied. Additionally, α_1 appears to increase with the third power of the frequency. Such frequency behaviour can be associated with Rayleigh scattering in two dimensions; it may be derived from first principles (Ishimaru 1978), or by reducing equation (18) to the Rayleigh limit and finding the frequency order of each term. The low frequency portions of the scattering coefficients in Fig. 4 exhibit similar frequency dependence.

As the title of this contribution suggests, a further study of elastic wave codas is being prepared for publication. Included in this later work will be the effects of shear modulus and anelasticity. I have also begun to use Nakamura's (1978) catalogue of lunar impacts for a more extensive study of the Moon's crustal inhomogeneities.

Acknowledgments

Bob Phinney germinated and found financial support for this research in the once fecund furrows of the National Aeronautics and Space Administration Lunar Sciences Program. I gratefully acknowledge Bob for his guidance and NASA for its unflagging support through Grant No. NSG-7080. For many of the ideas presented here, Tony Dahlen, Peter Leary and Jason Morgan have served as midwives, Neil Frazer, Richard Sterlitz and Steve Ward as sometimes unwilling witnesses. The reviews of two anonymous Referees were crucial ingredients in the preparation of the present manuscript.

References

Aki, K. & Chouet, B., 1975. Origin of coda waves: source attenuation and scattering effects, *J. geophys. Res.*, **80**, 3322–3343.

Aki, K., 1960. Study of earthquake mechanisms by a method of phase equalization applied to Rayleigh and Love waves, *J. geophys. Res.*, **65**, 729–740.

Anderson, D. L. & Archambeau, C. B., 1964. The anelasticity of the Earth, *J. geophys. Res.*, **69**, 2071–2084.

Andrianova, Z. S., Keilis-Borok, V. I., Levshin, A. L. & Neigauz, M. G., 1967. *Seismic Love Waves*, translated from Russian, Consultants Bureau, New York, 91 p.

Bugnolo, D. S., 1960. On the question of multiple scattering in the troposphere, *J. geophys. Res.*, **65**, 879–884.

Chernov, L. A., 1960. *Wave Propagation in a Random Medium*, McGraw-Hill, New York, 168 p.

Cooper, M. & Kovach, R., 1974. Lunar near surface structure, *Rev. Geophys. Space Phys.*, **12**, 291–308.

Dainty, A. M., Toksöz, M. N., Anderson, K. R., Pines, P. J., Nakamura, Y. & Lathum, G., 1974. Seismic scattering and shallow structure of the Moon in Oceanus Procellarun, *Moon*, **9**, 11–29.

Dainty, A. M. & Toksöz, M. N., 1977. Elastic wave propagation in a highly scattering medium – a diffusion approach, *J. Geophys.*, **43**, 375–388.

Ewing, M., Jardetzky, W. & Press, F., 1957. *Elastic Waves in Layered Media*, McGraw-Hill, New York, 380 p.

Frisch, U., 1968. Wave propagation in random media, in *Probabilistic Methods in Applied Mathematics*, ed. Bharaucha-Reid, A. T., Academic Press, New York, 291 p.

Herrera, I. & Mal, A. K., 1965. A perturbation method for elastic wave propagation 1, small inhomogeneities, *J. geophys. Res.*, **70**, 871–883.

Hudson, J., 1977. Scattered waves in the coda of *P*, *J. Geophys.*, **43**, 359–374.

Ishimaru, A., 1978. *Wave Propagation and Scattering in Random Media*, Academic Press, New York, 250 p.

Kennett, B. L. N., 1972. Seismic waves in laterally inhomogeneous media, *Geophys. J. R. astr. Soc.*, **27**, 301–325.

Kopnichev, Yu. F., 1977. The role of multiple scattering in the formation of a seismogram's tail, *Izv. Earth Phys.*, **13**, 394–398.

Landau, L. D. & Lifshitz, E. M., 1959. *Fluid Mechanics*, Pergamon Press, London, 536 p.

Malin, P. E., 1978. A first order scattering solution for modeling lunar and terrestrial seismic codas, *PhD Dissertation*, Princeton University.

Mark, N. & Sutton, G., 1975. Lunar shear velocity structure at Apollo sites 12, 14 and 15, *J. geophys. Res.*, **80**, 4940–4946.

Nakamura, Y., 1978. Sonograms of Lunar Codas, unpublished, University of Texas.

Pekeris, C. L., 1948. Theory of propagation of explosive sound waves in shallow water, *Geol. Soc. Am. Mem. 27*.

Saastamoinen, P. R., 1977. Modal approach to wave propagation in layered media with lateral inhomogeneities, *J. Geophys.*, **43**, 75–82.

Sato, H., 1977. Energy propagation including scattering effects – single isotropic scattering approximation, *J. Phys. Earth*, **25**, 27–41.

Tatarskii, V. I., 1971. The effects of the turbulent atmosphere on wave propagation, translated from Russian, National Technical Information Service, U.S. Dept. Com., T. T.-68-50464, Springfield, VA., 472 p.

Tolstoy, I., 1973. *Wave Propagation*, McGraw-Hill, New York, 466 p.

Woodhouse, J. H., 1974. Surface waves in laterally varying layered structure, *Geophys. J. R. astr. Soc.*, **37**, 461–490.

Appendix

As discussed in the text, the total scattered signal generated by an explosion or vertical impulse is proportional to the three line integrals (see step 5 of Basic Theory section).

$$\phi_1 = \int \frac{dx}{r} \exp(-\bar{\alpha}_m x - \bar{\alpha}_n r),$$

$$\phi_2 = \int \frac{dx}{r} \cos\theta \exp(-\bar{\alpha}_m x - \bar{\alpha}_n r), \tag{A1}$$

$$\phi_3 = \int \frac{dx}{r} \cos^2\theta \exp(-\bar{\alpha}_m x - \bar{\alpha}_n r).$$

The geometric relationships of r, x and θ are as shown in Fig. 1 and the condition $\bar{t}_{mnj} = 0$ allows r and θ to be expressed in terms of x:

$$r = g_n t - \gamma_{mn} x = \tau_n - \gamma_{mn} x,$$

$$\cos\theta = \frac{1}{2}\left[\frac{d^2}{xr} - \frac{x}{r} - \frac{r}{x}\right], \tag{A2}$$

$$\gamma_{mn} = \frac{g_n}{g_m}, \qquad \tau_n = g_n t.$$

Here γ_{mn} is the ratio of the incident and scattered wavelet group velocities and d is the station distance.

With equation (A2) the indefinite integral of equation (A1) can be completed, yielding algebraic, logarithmic, exponential and exponential integral quantities. For the contributions arising from $m \to m$ type events, $\bar{\alpha}_m(x + r) = \alpha_m g_m t$ and only algebraic, logarithmic and exponential terms occur. Whenever the diagonal selection rule is applicable, these terms

dominate and the ϕ become

$$\phi_1 = -(\ln r)\exp(-\bar{\alpha}_m\tau_m)$$

$$\phi_2 = \frac{1}{2}\left[\frac{d^2-\tau_m^2}{\tau_m r}+\frac{d^2+\tau_m^2}{\tau_m^2}\ln r+\frac{d^2-\tau_m^2}{\tau_m^2}\ln x\right]\exp(-\bar{\alpha}_m\tau_m)$$

$$\phi_3 = \frac{1}{4}\left[2\frac{d^4-\tau_m^4}{\tau_m^3 r}+\frac{(d^2-\tau_m^2)^2}{\tau_m^2 r^2}+\left(\frac{3d^4}{\tau_m^4}-\frac{2d^2}{\tau_m^2}+3\right)\ln r+\left(\frac{d^4}{\tau_m^3}-\frac{2d^2}{\tau_m}+\tau_m\right)\frac{1}{x}\right.$$
$$\left.+\left(\frac{3d^4}{\tau_m^4}-\frac{2d^2}{\tau^2}-1\right)\right]\exp(-\bar{\alpha}_m\tau_m). \qquad \text{(A3)}$$

The upper limit at which these quantities are to be evaluated is the maximum of x. This and the lower limit depend, in turn, on the definition of Π_q and the values of $\mathbb{k}_q$. Several relations are necessary to express the limits of x in terms of $\mathbb{k}_q$. These equations can best be presented by considering the upper limit of x as shown in the left half of Fig. 3(b). From Fig. 3(a), θ_1 is given by

$$\mathbb{k}_{q-1}^2 = k_1^2 + k_1^2 - 2k_1k_1\cos\theta_1. \qquad \text{(A4)}$$

Then, in terms of $\cos\theta_1$, x is a root of the quadratic form

$$(1+\gamma_{11}^2-2\gamma_{11}\cos\theta_1)x^2+2(\tau_1\cos\theta_1-\gamma_{11}^2\tau_1)x+(\tau_1^2-d^2)=0. \qquad \text{(A5)}$$

The second root of equation (A5) corresponds to the minimum value of x on the right hand side of Fig. 3(b). Equations (A4) and (A5) can be generalized by replacing the subscripts to correspond with the $m \to n$ event under consideration.